The compact UV Nucleus of M33

Dubus, G.M.B.; Charles, P.A.; Long, K.S.

Published in:
Astrophysical Journal

DOI:
10.1086/312113

THE ASTROPHYSICAL JOURNAL, 519:L135–L138, 1999 July 10

THE COMPACT UV NUCLEUS OF M33

GUILLAUME DUBUS
Astronomical Institute "Anton Pannekoek," University of Amsterdam, Kruislaan 403, 1098 SJ Amsterdam, Netherlands
KNOX S. LONG
Space Telescope Science Institute, 3700 San Martin Drive, Baltimore, MD 21218
AND
PHILIP A. CHARLES
Department of Astrophysics, University of Oxford, Keble Road, Oxford OX1 3RH, England, UK
Received 1999 January 7; accepted 1999 May 6; published 1999 June 4

ABSTRACT

The most luminous X-ray source in the Local Group is associated with the nucleus of M33. This source, M33 X-8, appears modulated by ~20% over a ~106 day period, making it unlikely that the combined emission from unresolved sources could explain the otherwise persistent ~10^{39} ergs s^{-1} X-ray flux. We present here high-resolution UV imaging of the nucleus with the Planetary Camera of the *Hubble Space Telescope* undertaken in order to search for the counterpart to X-8. The nucleus is bluer and more compact than at longer wavelength images, but it is still extended, with half of its 3×10^{38} ergs s^{-1} UV luminosity coming from the inner 0.″14. We cannot distinguish between a concentrated blue population and emission from a single object.

Subject headings: galaxies: individual (M33) — galaxies: nuclei — Local Group — ultraviolet: stars

1. INTRODUCTION

The nearby galaxy M33 hosts the most luminous steady X-ray source in the Local Group, X-8. This source, with $L_X \sim 10^{39}$ ergs s^{-1} (Long et al. 1996), is coincident to within 5″ with the nucleus of the galaxy (Schulman & Bregman 1995). Different models were invoked for X-8, including a quiescent mini–active galactic nucleus (Trinchieri, Fabbiano, & Peres 1988; Peres et al. 1989), a collection of X-ray binaries (Hernquist, Hut, & Kormendy 1991), and a new type of X-ray binary (Gottwald, Pietsch, & Hasinger 1987). Our *ROSAT* studies (Dubus et al. 1997) have shown that X-8 is very steady on both short and long timescales, except for low-amplitude (~20%) variations, which appear modulated on a ~106 day period. This strongly favors a single-source explanation for X-8.

We have interpreted the modulation in X-8 as "superorbital," similar to that seen in a number of bright Galactic X-ray binaries that were monitored by, e.g., the *Vela 5B* satellite (Smale & Lochner 1992). X-8 is then likely to be a $\geq 10\ M_\odot$ black hole X-ray binary (the high mass is required to account for the observed luminosity) but with a companion in an orbital period much shorter than 106 days. This is supported by the extremely low velocity dispersion of the nucleus, which limits the mass of a central black hole in M33 to $\leq 5 \times 10^4\ M_\odot$ (Kormendy & McClure 1993, hereafter KM93). This and the high central stellar density imply that the nucleus is an extremely relaxed, post–core-collapse stellar system (comparable, for instance, to a Galactic globular cluster such as M15). A significant number of stellar collisions/interactions could have taken place, eventually leading to the creation of exotic interacting binaries (e.g., Hut et al. 1992).

The next step toward unraveling the mystery of X-8 would be to identify its optical counterpart. However, even with optimistic L_X/L_{opt} ratios for either X-ray binaries or active galactic nuclei, the counterpart would only have $V \sim 21$ compared to a core brightness of $V \sim 14$. But with the optical spectral type of an F supergiant, the dominance of the M33 visual core cannot extend to UV wavelengths at which the hot/flat spectrum of X-8's associated disk ought to be a significant contributor. This is true despite evidence for a color gradient in the nucleus (KM93; Mighell & Rich 1995; Lauer et al. 1998), suggesting that a period of recent star formation has taken place and/or that collisions have modified the central star population. Here we report an attempt to find the counterpart using the UV imaging capabilities of the *Hubble Space Telescope* (*HST*).

2. OBSERVATIONS AND REDUCTION

Observations were carried out with the *HST* Wide Field Planetary Camera 2 (WFPC2) on 1997 June 12 using three different filters. The nucleus was positioned at the center of the Planetary Camera (PC; $\alpha = 1^h33^m51\overset{s}{.}1$, $\delta = 30°39'39''$ [J2000]). During the first orbit, two 1200 s exposures were made with the F160BW (UV filter, $\bar{\lambda} = 1491$Å). In the following orbit, two 800 s exposures were made with the F300W filter (*U* filter, $\bar{\lambda} = 2942$Å) and one 500 s exposure with the F439W filter (*B* filter, $\bar{\lambda} = 4300$Å). All these exposures were made with the gain setting at 7.

In addition, we have extracted recalibrated archival data from the Space Telescope European Coordinating Facility Archive. These data included two 40 s exposures with the F555W at gain 14 (*V* filter, $\bar{\lambda} = 5397$Å), two 40 s exposures with the F814W at gain 14 (*I* filter, $\bar{\lambda} = 7924$Å), and six 300 s exposures with the F1042M at gain 7 ($\bar{\lambda} = 10190$Å) filters, all centered on the nucleus and dating from 1994 September 26–27. The archival *V* and *I* data were previously discussed by Lauer et al. (1998, hereafter L98). Figure 1 shows the central region of the reduced UV, *U*, and *B* images.

The data were reduced using the *HST* calibration pipeline (Biretta et al. 1996). The signal-to-noise ratio of the only existing F160BW flat field was quite low. Following advice from the WFPC2 group at STScI, we decided to use the F255W flat field. Effects of cosmic rays were reduced on those images for which we had multiple exposures with the IRAF STSDAS routine CRREJ. Images of the nuclear region as observed through the F160BW, F300W, and F439W filter with the PC are shown in Figure 1.

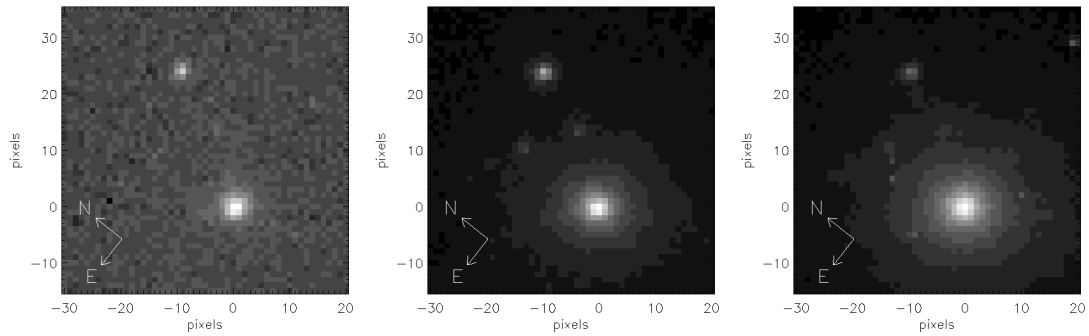

FIG. 1.—Central portion of the Planetary Camera showing the nucleus and the nearby star in the F160BW UV (*left*), F300W *U* (*middle*), and F439W *B* filters (*right*). Each pixel is 0.″0455, i.e., each image is about 2.″3 × 2.″3.

3. ANALYSIS

Our values for the total flux of the nucleus in the different bands agree with those of Gordon et al. (1999). The radial profiles of the *B*, *V*, and *I* data are also consistent with KM93 and L98. As is apparent from Figure 1, the nucleus of M33 appears more concentrated in the F160BW filter than in the longer-wavelength filters. Nevertheless, as shown in Figure 2, the profile in the F160BW image of the nucleus is extended compared to the profile of the star located about 1″ north-northwest from the nucleus and to point-spread function (PSF) profiles calculated using the *HST* PSF-generating routine TinyTim[1] (Krist & Hook 1997). Further investigation of the radial structure of the UV emission calls for deconvolution of the data taking into account the different instrumental effects in the Planetary Camera (L98). Since the UV image does not have a large enough signal-to-noise ratio to allow for a proper deconvolution, we chose instead to fit convolved models to the data.

3.1. *Fits of Extended Emission Models*

Following KM93, we fitted radial profile models of the form

$$\Sigma = \Sigma_0 [1 + (r/r_0)^2]^{-n} . \quad (1)$$

[1] Available at http://scivax.stsci.edu/~krist.tinytim.html.

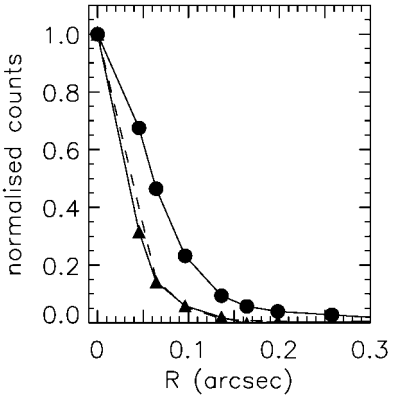

FIG. 2.—Radial profiles of the nucleus and nearby star in UV. The nucleus is shown by the filled circles and continuous line. The star north-northwest of the nucleus (see Fig. 1) is shown by the triangles and continuous line. The best-fitting PSF to the star is shown by the dashed line. The nucleus in UV is clearly extended.

The model and the PSF are oversampled on a 4 × 4 grid for each PC pixel. For a given set of (r_0, n), the convolved model is moved on the 4 × 4 grid, rebinned to the PC resolution, and compared to the data. The comparison with the data is performed in a 64 × 64 pixel aperture (about 3″ × 3″), but we have verified that larger and smaller apertures gave similar results. We have assumed an A-type spectrum for the PSF, but other choices do not affect our conclusions. The parameter r_0 is varied between 0.05 and 2 PC pixels, and n is varied between 0.5 and 2. The results from the χ^2 minimization routine are presented in Table 1 and Figure 3. The quoted errors correspond to 10% higher values than at the minimum of the fit function. In the noisy UV band, only lower bounds to the parameters could be extracted. Here we give errors on the FWHM instead of on r_0.

The FWHM of the models decreases in accordance with the blue color gradient. In all cases $n \approx 1$, suggesting that the distribution of light at large radii is the same in all the filters. This is consistent with the flat color profiles observed for $r \gg r_0$. With n fixed at 0.75 as in L98, we also find a FWHM for the F555W data of 0.″07. This is clearly not the best solution when n varies (Table 1). We find a higher FWHM (0.″09). We note that KM93 find n between 0.8 and 1.3 and a FWHM below 0.″1. The similar values found for r_0 in the *V*, *I*, F1042M, and (to a lesser extent) *B* bands indicate that their radial profiles are comparable (i.e., the color gradients are much reduced between those bands than when compared to the UV and *U* so that, for example, on first approximation the $V-I$ color gradient is negligible when compared to UV$-V$).

3.2. *Fits with an Additional Point Source*

Since the *V*, *I*, and F1042M bands show very close light distributions, we investigated whether the compact emission from the UV and *U* filter could be explained by an underlying extended population having the *V*-band distribution plus a blue point source. We fixed $r_0 = 1$ PC pixel and $n = 1$ and superposed at the center of this model a point source of varying

TABLE 1
FITS OF EXTENDED EMISSION MODELS

Filter	r_0 (PC pixel)	n	FWHM (0.″001)
F160BW	0.4	$1.1_{-0.2}$	35_{-25}
F300W	0.5	$1.0^{+0.2}_{-0.1}$	45^{+25}_{-15}
F439W	0.8	$1.0^{+0.1}_{-0.1}$	75^{+20}_{-15}
F555W	1.0	$1.0^{+0.05}_{-0.05}$	90^{+15}_{-5}
F814W	0.9	$0.9^{+0.1}_{-0.05}$	90^{+15}_{-15}
F1042M	1.0	$0.9^{+0.1}_{-0.1}$	100^{+15}_{-25}

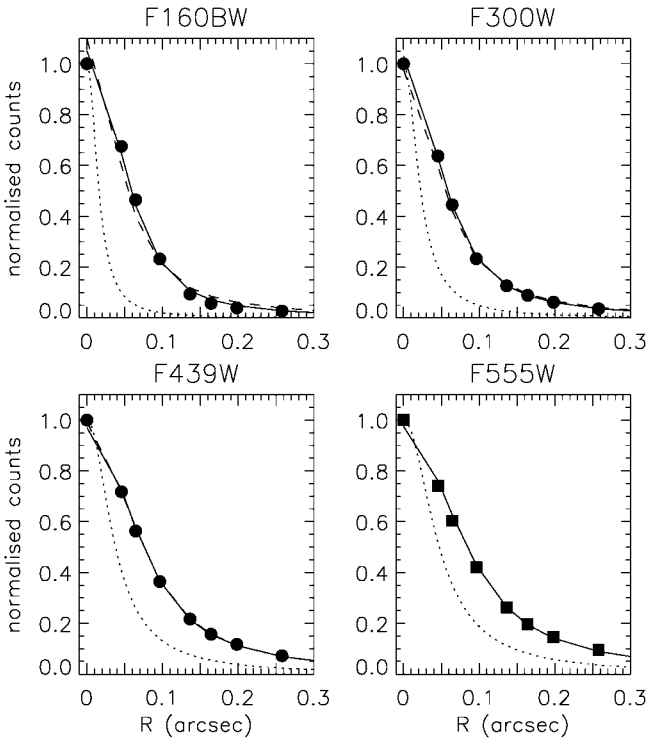

FIG. 3.—Radial profiles of the nucleus in the different filters (*data points*). The best-fitting PSF convolved models assuming only extended emission (§ 3.1) are shown by straight lines. The unconvolved models (eq. [1]) are shown as dotted lines. PSF convolved models assuming extended emission and a point source (§ 3.2) are shown with dashed lines in the F160BW (UV), F300W (*U*), and F439W (*B*) profiles. Normalization factors are (in mag arcsec^{-2}) 11.67 (F160BW), 11.65 (F300W), 12.10 (F439W), and 11.76 (F555W).

relative strength. For the *V* and redward filters, the best fits were consistently obtained with a nil contribution from the point source. However, a point source of increasing strength was needed in *B*, *U*, and UV. Only those models with fit values within the errors of the previous extended emission fits (Table 1) were kept, i.e., the fits here are as good or better than the previous ones (see Fig. 3). The contribution of the point source to the total flux within a 1.″45 circular aperture is summarized in Table 2. The corresponding magnitudes are given in the VegaMAG system using updated tables for the zero points (Holtzman et al. 1995).

The best fits for the *B*, *U*, and UV bands are shown in Figure 3 by dashed lines. They are indistinguishable from the extended emission fits. As a result we cannot, based on the data in hand, distinguish between a model in which emission is extended in the UV but has a smaller core radius than at longer wavelengths and a composite model consisting of a point source and an underlying distribution characterized by the visible light profile.

4. DISCUSSION

The nucleus of M33 has a composite spectrum ranging from A7 V at $\lambda \sim 3800$ Å to F5 V at $\lambda \sim 4300$ Å (O'Connell 1983). This requires at least a two-component population in most models, with the blue emission being due to young metal-rich stars. The color gradient in $B-R$ implies that this young population is more centrally condensed. The nucleus could have been the site of episodic starbursts with the youngest stars being about 10 Myr old (O'Connell 1983; van den Bergh 1991; Schmidt, Bica, & Alloin 1990; and references therein). Recently, Gordon et al. (1999) have argued that a single 70 Myr old starburst reproduces the UV-to-IR spectral energy distribution within 4.″5 of the center if dust is correctly taken into account.[2] The nucleus is also very similar to a globular cluster and is likely to have undergone core collapse (Hernquist et al. 1991; KM93). Blue stars formed in collisions at the center might explain the color gradient. This model may have difficulties accounting for the UV luminosity (Hernquist et al. 1991; L98; Gordon et al. 1999).

TABLE 2
FITS WITH ADDITIONAL POINT SOURCE

Filter	Point-Source Flux (%)	Magnitude (VegaMAG)
F160BW	18^{+4}_{-3}	16.9
F300W	8^{+4}_{-2}	17.5
F439W	1^{+2}_{-1}	19.7

NOTE.—Values given are within a 1.″45 aperture.

Massey et al. (1996) detected the nucleus in the UV, but with 5″ resolution. Hence, they had proposed that the blue component of the nucleus could be due to unresolved emission from a few hot stars. However, the *HST* data shows that the UV emission is very compact, with no stars of comparable brightness within 5″ of the center. The total flux is about 6.3×10^{-15} ergs s^{-1} cm^{-2} Å^{-1} in a 4.″55 aperture or about 2.8×10^{38} ergs s^{-1} at 800 kpc. From the best-fit model, ~50% of the UV light comes from the inner 0.″14 of the nucleus. Any model of the structure of the nucleus has to explain this UV emission from a region only ~0.55 pc across. If a point source is present, this source is responsible for ~30% of the UV flux within 0.″14. The contribution from the underlying extended population is subsequently reduced.

The nucleus of NGC 205, at a comparable distance of 720 kpc, is in many ways similar to that of M33, but without the X-ray source. It is globular cluster–like and has a comparable M_V and a low upper limit of $9 \times 10^4\ M_\odot$ on the mass within the central parsec (Heath Jones et al. 1996). These authors find that the nucleus is more extended, with a F555W FWHM of 0.″2, $F_{\rm F555W} = 1.8 \times 10^{-15}$ ergs s^{-1} cm^{-2} Å^{-1}, and only $F_{\rm F160BW} = 6.0 \times 10^{-16}$ ergs s^{-1} cm^{-2} Å^{-1} (within 0.″273). Using the same aperture on the M33 data, we find for M33 $F_{\rm F555W} = 3.4 \times 10^{-15}$ and $F_{\rm F160BW} = 2.5 \times 10^{-15}$ ergs s^{-1} cm^{-2} Å^{-1}. Excluding the contribution from the point source, the F160BW flux of M33 is about 1.5×10^{-15} ergs s^{-1} cm^{-2} Å^{-1} and the ratios of the fluxes between the bands become comparable.

If there is in fact a point source at the center of the nucleus of M33, the magnitude estimates in Table 2 are consistent with a Rayleigh-Jeans tail. We estimate that the total UV flux of the source would be $\sim 1.0 \times 10^{-15}$ ergs s^{-1} cm^{-2} Å^{-1}, which would suggest $L_{\rm opt}/L_{\rm X} \sim 0.05$, a reasonable value for the type of X-ray source we have postulated X-8 to be. This source would be responsible for most of the color gradient in UV$-B$ and $U-B$ and thus the very compact appearance of the nucleus at these wavelengths. Since it contributes only ~18% of the total F160BW flux and ~8% of the F300W flux, the spectral energy distribution of the nucleus is not changed much and the consequences on population synthesis studies should be minor. However, it does have a major influence in that it relaxes the constraints on, e.g., mass segregation to explain the very strong color gradients in UV$-B$ and $U-B$.

[2] Gordon et al. (1999) propose that X-8 is a high-mass X-ray binary with an early-B companion. But as had been noted by O'Connell (1983), the high mass transfer rate needed to power the 10^{39} ergs s^{-1} luminosity implies an uncomfortably short evolutionary timescale (~10^5 yr).

The star located about 1″ from the nucleus in M33 has $B = 19.45$, $V = 19.25$, $M_{F300W} = 18.05$, and $M_{F160BW} = 17.60$. The count rates are compatible with an A0-type spectrum, which would make it similar, although fainter, to the two A supergiants detected by Massey et al. (1996). The fluxes in the F300W and F160BW bands, at the distance of M33 (~800 kpc), are $\sim 10^{37}$ ergs s^{-1}. The positional accuracy of the *ROSAT* HRI does not rule out this star as a possible counterpart to the X-ray source X-8. The ratio $L_X/L_{opt} \sim 100$ and the observed $U-B$ and $B-V$ would agree with what is expected from a low-mass X-ray binary (van Paradijs & McClintock 1995). But its absolute magnitude ($M_V \approx -5.2$) would make it more similar to a high-mass X-ray binary. The main argument against this star being the X-ray binary is X-8's unique character and special location at the nucleus. Given that Massey et al. (1996) found ~300 analogous UV sources in M33, it would be remarkable that the one near the nucleus is the most luminous X-ray source in the Local Group.

5. CONCLUSION

The UV high-resolution images obtained with the *HST* Planetary Camera show that the nucleus of M33 is extremely compact. We have fitted convolved models to the radial profiles in the different bands from which we find the FWHM of the nucleus in UV to be ~0.″035 and ~0.″090 in *V*. About half of the UV flux comes from the inner 0.″14 of the nucleus. The UV and *U* profiles are also well fitted if one assumes a blue point source superposed on an extended population with the same FWHM as in *V*. If this is the correct model for the nucleus, then this point source is likely to be the UV counterpart to the very luminous X-ray source X-8. Such a counterpart would be responsible for most of the strong color gradient seen to UV. Its contribution to the total UV flux of the nucleus would be about 18%. Models for the structure of the nucleus still need to account for the remainder of the UV flux, but the constraints on population segregation (more compact blue star population) are reduced. High spatial resolution UV spectroscopy of the nucleus is the obvious next step, which we will undertake shortly.

We thank Sylvia Baggett for help with the F160BW filter reduction. G. D. and K. S. L. wish to thank the Oxford Astrophysics Department, where part of this work was completed. We acknowledge support by the British-French joint research program *Alliance* and by NASA grant NAG5-1539 to the STScI. Based on observations with the NASA/ESA *Hubble Space Telescope* obtained at the STScI, which is operated by AURA under NASA contract NAS5-26555.

REFERENCES

Biretta, J. A., et al. 1996, The WFPC2 Instrument Handbook, Version 4.0 (Baltimore: STScI)
Dubus, G., Charles, P. A., Long, K. S., & Hakala, P. J. 1997, ApJ, 490, 47
Gordon, K. D., Hanson, M. M., Clayton, G. C., Rieke, G. H., & Misselt, K. A. 1999, ApJ, in press
Gottwald, M., Pietsch, W., & Hasinger, G. 1987, A&A, 175, 45
Heath Jones, D., et al. 1996, ApJ, 466, 742
Hernquist, L., Hut, P., & Kormendy, J. 1991, Nature, 354, 376
Holtzman, J. A., Burrows, C. J., Casertano, S., Hester, J. J., Trauger, J. T., Watson, A. M., & Worthey, G. 1995, PASP, 107, 1065
Hut, P., et al. 1992, PASP, 104, 981
Kormendy, J., & McClure, R. D. 1993, AJ, 105, 1793 (KM93)
Krist, J., & Hook, R. 1997, The TinyTim User's Guide, Version 4.4
Lauer, T. R., Faber, S. M., Ajhar, E. A., Grillmair, C. J., & Scowen, P. A. 1998, AJ, 116, 2263 (L98)
Long, K. S., Charles, P. A., Blair, W. P., & Gordon, S. M. 1996, ApJ, 466, 750
Massey, P., Bianchi, L., Hutchings, J. B., & Stecher, T. P. 1996, ApJ, 469, 629
Mighell, K. J., & Rich, R. M. 1995, AJ, 110, 1649
O'Connell, R. 1983, ApJ, 267, 80
Peres, G., Reale, F., Collura, A., & Fabbiano, G. 1989, ApJ, 336, 140
Schmidt, A. A., Bica, E., & Alloin, D. 1990, MNRAS, 243, 620
Schulman, E., & Bregman, J. N. 1995, ApJ, 441, 568
Smale, A. P., & Lochner, J. C. 1992, ApJ, 395, 582
Trinchieri, G., Fabbiano, G., & Peres, G. 1988, ApJ, 325, 531
van den Bergh, S. 1991, PASP, 103, 609
van Paradijs, J., & McClintock, J. E. 1995, in X-Ray Binaries, ed. W. H. G Lewin, J. van Paradijs, & E. P. J. van den Heuvel (Cambridge: Cambridge Univ. Press), chap. 2